Carbon 201 (2023) 712–718

Contents lists available at ScienceDirect

Carbon

journal homepage: www.elsevier.com/locate/carbon

A method to estimate adhesion energy of as-grown graphene in a roll-to-roll dry transfer process

Nan Hong [a,1], Qishen Zhao [a,1], Dongmei Chen [a], Kenneth M. Liechti [b], Wei Li [a,*]

[a] Walker Department of Mechanical Engineering, University of Texas at Austin, 204 E. Dean Keeton St., Austin, TX, 78712-1591, United States
[b] Department of Aerospace Engineering and Engineering Mechanics, University of Texas at Austin, 2617 Wichita Street, Austin, TX, 78712-1221, United States

ARTICLE INFO

Keywords:
CVD graphene
Roll-to-roll dry transfer
Adhesion energy
Web bending

ABSTRACT

The interfacial adhesion energy of as-grown graphene on its metal growth substrate is an important variable in designing, monitoring, and controlling a roll-to-roll (R2R) graphene transfer process using mechanical peeling. In this study, we develop a novel method to estimate the adhesion energy of as-grown graphene during the R2R dry transfer process. An energy balance model is established to derive the adhesion energy based on web tension and bending curvature measurements. Experiments were conducted under various mechanical peeling conditions. The adhesion energy of as-grown graphene on copper foil was determined to be from 1.22 J/m^2 to 2.58 J/m^2 depending on the peeling front geometry. The developed adhesion energy estimation method is compatible with the R2R process and can be used to monitor and control the large-scale graphene transfer process with in-process measurements.

1. Introduction

Graphene grown on catalytic metal via chemical vapor deposition (CVD) has been envisioned for many advanced applications such as wearable electronics, solar cells, and flexible displays [1–5]. Large-scale graphene growth on copper and nickel has been demonstrated using a roll-to-roll (R2R) CVD process [6,7]. After the growth, CVD graphene needs to be transferred from its growth substrate to a target substrate for device fabrication. A R2R dry transfer system was recently developed based on mechanical peeling [8–11]. Compared with the wet transfer processes [12–15], the mechanical peeling process is fast and environmentally benign and does not leave undesirable chemical residues on the transferred graphene. Furthermore, the dry transfer process allows reuse of the metal substrate for graphene growth, reducing the overall fabrication cost.

In a R2R dry transfer system, the interfacial adhesion energy between the as-grown graphene and its growth substrate is an important parameter that needs to be determined for designing, monitoring, and controlling the mechanical peeling process. Until now, the adhesion energy of as-grown graphene has been measured using different techniques. Yoon et al. [16] was among the earliest to use a double cantilever beam (DCB) setup to measure the adhesion energy. The adhesion energy of monolayer graphene synthesized on a copper substrate was determined to be 0.72 ± 0.07 J/m^2. With a similar setup, Na et al. reported the adhesion energy between 1.54 ± 0.07 J/m^2 [17] and 6.0 J/m^2 [18] depending on the rate of separation. A nano-scratch technique was developed by Das et al. [19], yielding an adhesion energy value of 12.8 J/m^2 for graphene grown on copper. Such a high value might be caused by the substantial plastic deformation of copper during the nano scratch process. Based on a standard blister testing technique [20], Hao et al. [21] developed a method to determine the adhesion energy of as-grown graphene on copper and found it to be 0.74 ± 0.13 J/m^2, 1.10 ± 0.16 J/m^2, and 1.53 ± 0.1 J/m^2 due to the difference in surface roughness levels of the copper substrate.

As can be seen, all the above techniques for adhesion energy measurement relied on special configurations and procedures that are not compatible with the R2R process. More importantly, previous studies all focused on a quasi-static measurement method that cannot be used for in-process adhesion energy estimation. As the adhesion energy could vary due to process conditions such as peeling angle and peeling speed, a method to estimate the adhesion energy during the R2R mechanical peeling process is needed for monitoring and controlling the R2R dry transferred graphene. In this study, we develop a novel approach to determining the adhesion energy of as-grown graphene using real-time

* Corresponding author.
E-mail address: weiwli@austin.utexas.edu (W. Li).
[1] These authors contributed equally to this work.

https://doi.org/10.1016/j.carbon.2022.08.062
Received 13 June 2022; Received in revised form 13 August 2022; Accepted 17 August 2022
Available online 26 August 2022

in-process measurements. An energy balance model is developed that includes the web bending effect in the R2R process. Experiments were conducted with graphene-on-copper samples of different sizes to introduce various adhesion force conditions. To our knowledge, this is the first study to report the adhesion energy of as-grown graphene with a R2R configuration. It provides a method to estimate a key process variable that can be used for monitoring and control of the large-scale graphene transfer process.

2. Energy balance in a R2R dry transfer process of graphene

For R2R dry transfer of graphene, a layer of polymer is first laminated onto graphene on metal foil. The laminate is then sandwiched between two carrier films and loaded on an unwinding roller. After peeling, graphene is transferred to the polymer film and collected by a rewinding roller. The metal foil is collected by another rewinding roller. Fig. 1 shows a schematic of the R2R dry transfer process. Fig. 1(a) shows that the incoming laminate is peeled with two guiding rollers, whose radius is denoted as R. The unwinding roller speed is denoted as and the linear film speeds before and after peeling are denoted as V_1, V_2 and V_3, respectively. Correspondingly, the tension forces are denoted as T_1, T_2, and T_3 and the resulting elastic strains in each of the films as ε_1, ε_2 and ε_3, respectively. Fig. 1(a) also shows the composition of the web sections before and after peeling. The sample preparation and loading procedure will be described later in the experimental setup section. Fig. 1(b) shows geometric configuration of the peeling front. The peeling angle θ is defined as the angle between T_2 and T_3. The angle α is defined as the angle between tensions T_1 and T_2. The extension line of T_1 further divides the peeling angle into θ_1 and θ_2.

For the peeling process to be feasible, the energy release rate G of the peeling action should be equal to the adhesion energy Γ. The adhesion energy Γ characterizes the bonding strength between the two materials at the interface. Zhao et al. [10] derived the energy release rate in a R2R mechanical peeling process based on three energy terms. As shown in Fig. 2(a), these three terms of energy included the energy dissipated due to the creation of a new interface area (U_1), the potential energy change due to the work done by the external forces (U_2), and the elastic potential energy due to the change of strains in the films during the peeling process (U_3). Consider that a small peeling length Δd_1 is created under tensions T_1, T_2 and T_3 with peeling angles θ_1 and θ_2. The energy dissipated due to the creation of a new interface area U_1 can be expressed as

$$U_1 = -\Gamma b \Delta d_1 \tag{1}$$

where b is the width of the web. The potential energy changes due to the work done by the external forces U_2 can be defined as

$$U_2 = T_2 \Delta d_1 (1 - \cos\theta_2 + \varepsilon_2 - \varepsilon_1) + T_3 \Delta d_1 (1 - \cos\theta_1 + \varepsilon_3 - \varepsilon_1) \tag{2}$$

The elastic potential energy due to the change of strain in the films during the peeling process U_3 is given by

$$U_3 = \frac{1}{2}\frac{b h_{f2} \Delta d_1}{(1+\varepsilon_1)} E_2 \left(\varepsilon_1^2 - \varepsilon_2^2\right) + \frac{1}{2}\frac{b h_{f3} \Delta d_1}{(1+\varepsilon_1)} E_3 \left(\varepsilon_1^2 - \varepsilon_3^2\right) \tag{3}$$

where h_{f2} and h_{f3} are the thicknesses and E_2 and E_3 are the elastic moduli of the corresponding web section.

The above formulation did not consider the web bending effect in the R2R mechanical peeling process. In reality, however, all three web sections before and after the peeling point will bend due to the complex force balance condition in the peeling process. A more realistic peeling front geometry is shown in Fig. 2(b). The curvature due to bending of the unpeeled section is denoted as K_1, and those of the peeled sections are denoted as K_2 and K_3, respectively. According to He et al. [22], the bending effect of a hyper-elastic film in a mechanical peeling process is substantial, and the bending energy can be expressed as

$$U_b = \frac{\Delta d_1}{2} E_b I_b {K_b}^2 \tag{4}$$

where K_b is the curvature, E_b is the elastic modulus, and I_b is the moment of inertia of the film. When a new surface is created, the curvature of the unpeeled web section is changed from K_1 to K_2 and K_3 after peeling. Therefore, the potential energy changes due to bending during the peeling process can be expressed as

$$U_4 = \frac{\Delta d_1}{2}\left[E_2 I_2 \left({K_1}^2 - {K_2}^2\right) + E_3 I_3 \left({K_1}^2 - {K_3}^2\right)\right] \tag{5}$$

where the subscripts indicate the web sections as shown in Fig. 2. Based on energy conservation, which requires $\Sigma U_i = 0$, for $i = 1$ to 4, the adhesion energy can then be obtained as

$$\begin{aligned}\Gamma = {} & \frac{T_3}{b}(1 - \cos\theta_1 + \varepsilon_3 - \varepsilon_1) + \frac{T_2}{b}(1 - \cos\theta_2 + \varepsilon_2 - \varepsilon_1) \\ & + \frac{1}{2}\frac{b h_{f2} \Delta d_1}{(1+\varepsilon_1)} E_2 \left(\varepsilon_1^2 - \varepsilon_2^2\right) + \frac{1}{2}\frac{b h_{f3} \Delta d_1}{(1+\varepsilon_1)} E_3 \left(\varepsilon_1^2 - \varepsilon_3^2\right) + \frac{1}{2b}\left[E_2 I_2 \left({K_1}^2 - {K_2}^2\right)\right. \\ & \left. + E_3 I_3 \left({K_1}^2 - {K_3}^2\right)\right]\end{aligned} \tag{6}$$

Unlike classic adhesion mechanics formulation, the above energy balance model considers the R2R peeling geometry, strain energy stored

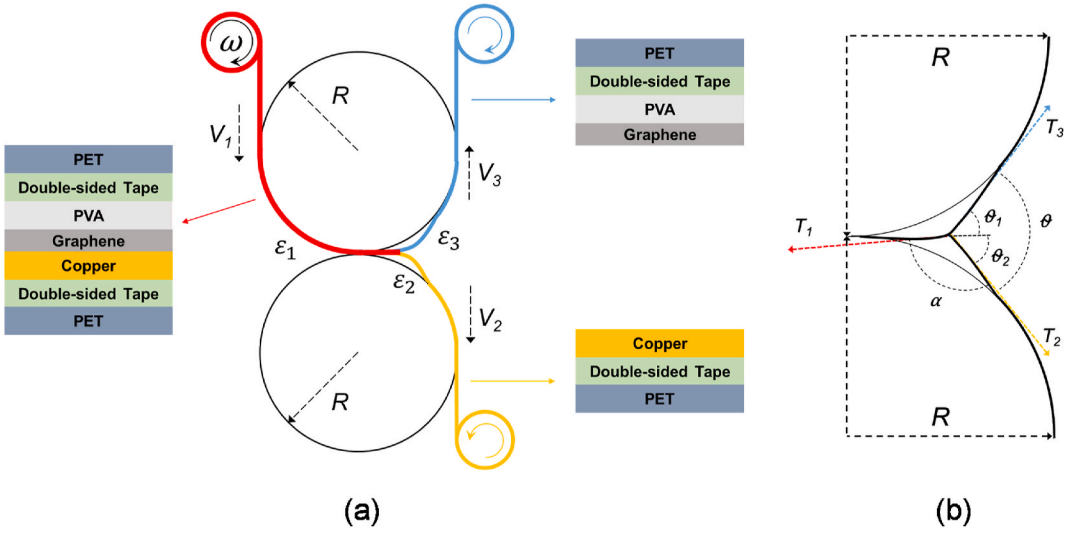

Fig. 1. (a) Schematic of a R2R peeling process. (b) A detailed view of the peeling front geometry. (A colour version of this figure can be viewed online.)

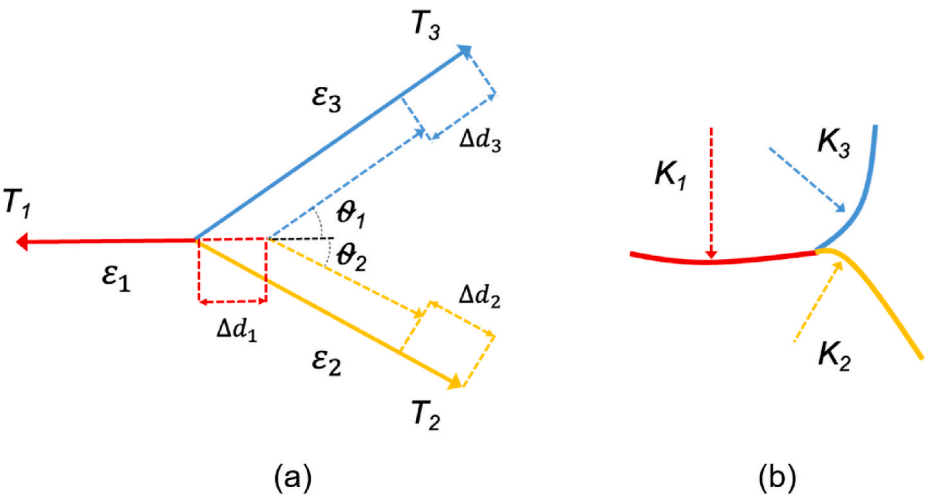

Fig. 2. (a) Schematic of a R2R peeling process without bending, (b) bending of the web sections during the R2R process. (A colour version of this figure can be viewed online.)

in flexible substrates, and the film bending effect during the peeling process. The angles in the above equations θ and α can be determined based on the force balance equations below [10].

$$T_2 + T_3 \cos\theta + T_1 \cos\alpha = 0 \tag{7}$$

$$T_1 \sin\alpha = T_3 \sin\theta \tag{8}$$

where

$$\theta = \theta_1 + \theta_2 \tag{9}$$

$$\alpha = \pi - \theta_2 \tag{10}$$

3. Experimental setup

Experiments were conducted on a lab built R2R testbed as shown in Fig. 3. The unwinding roller was driven by a NEMA 23 stepper motor (1-DM542S–23HS45), while the rewinding rollers were driven by two brushless DC motors (Aerotech BM130). Three of the idler rollers were instrumented with cantilevered load cells (MAGPOWR CL-1-50) to measure web tensions. A digital camera was used to measure the film bending during the R2R peeling process. Two feedback controllers were implemented to track the tension set-points of T_2 and T_3 independently. The web speed at the unwinding roller was controlled by the stepper motor. Both tension forces T_2 and T_3 were set at 5 N in this study. The linear speed of peeling was fixed at 1.0 m/min.

The graphene samples used in this study were CVD-grown monolayer graphene on copper foil (25 μm thickness) from Grolltex, CA. As-received graphene-on-copper sheets were cut into smaller samples to reduce the material cost of the experiment. The sample size across the peeling direction, defined as sample width, was varied from 2 cm to 10 cm. The sample size along the peeling direction was fixed at 1 cm. The samples were first coated with polyvinyl alcohol (PVA, Mw 9000–10,000 g/mol, 80% hydrolyzed) solution and dried in a vacuum oven. Coated samples were then sandwiched between two rolls of polyethylene terephthalate (PET) carrier film (MYLAR® A, 100 μm thick) with double-sided pressure-sensitive tape (Scotch Tape 6137H). Fig. 4 shows a schematic of the composite structure of the samples after loading onto the carrier films. The sample size and material property parameters are listed Table 1. Based on the equivalent area method [23], the equivalent flexural rigidity of each web (E_2I_2 and E_3I_3) of the composite beams can be determined for graphene-on-copper samples of different widths (see Supplementary Table S1).

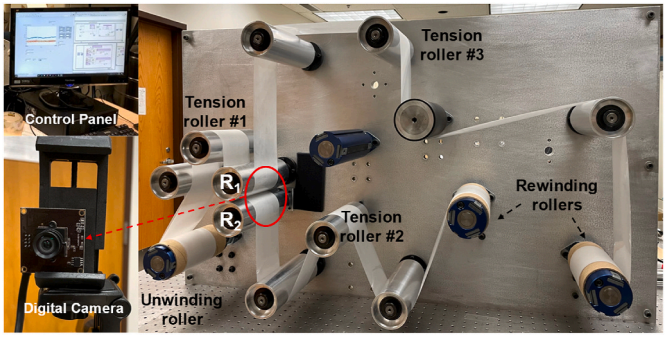

Fig. 3. The R2R mechanical peeling system. (A colour version of this figure can be viewed online.)

4. Results and discussion

4.1. Tension monitoring and adhesion energy estimation

The results from a R2R dry peeling experiment with a graphene sample of 8 cm wide are shown in Fig. 5. To confirm the successful graphene transfer, Raman spectroscopy and scanning electron microscopy were used to inspect the peeled graphene-on-PVA sample, and the results are shown in Supplementary Fig. S2. Fig. 5(a) is a series of still images showing the peeling front progression as the graphene sample going through the peeling process. During the peeling process, the carrier films were pulled away from the guiding roller surface, causing further bending of the web sections. Fig. 5(b) shows the corresponding tension force measurements on the three sections of the web. In the R2R system, the film tensions T_2 and T_3 were controlled by automatic controllers. Although the initial tensions T_2 and T_3 were set at 5 N, the tension forces would change due to the peeling action. As shown in Fig. 5 (b), the peeling tensions can be divided into four regions of interest. In region A, the tension forces increase to build up enough strain energy for the peeling process to start. Once the peeling process begins, the tension forces start to drop as shown in region B, with T_2 drops more significantly than T_3 and T_1. The sudden drop of T_2 easily marks the starting point of the peeling process. Region C is the period when the peeling front geometry and tension forces remain relatively stable. After the peeling process is complete, the stretching and bending of the film is suddenly released, resulting in sudden drops and oscillations in the tension forces, as seen in region D. For comparison, tension measurements without the peeling action are shown in Fig. S3.

Fig. 5(c) shows the real-time adhesion energy estimate during the

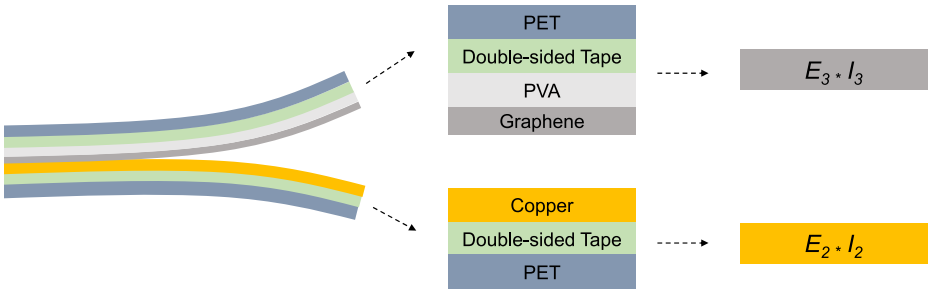

Fig. 4. The composite sample structure in the R2R graphene peeling process. (A colour version of this figure can be viewed online.)

Table 1
Parameters used in the experiment.

Parameters	Value
$E_{PET\ film}$	2.7 GPa
$E_{Copper\ film}$	121 GPa
E_{tape}	1.8 GPa
$E_{PVA\ film}$	0.7 GPa
$h_{PET\ film}$	100 μm
$h_{copper\ film}$	25 μm
h_{tape}	60.96 μm
$h_{PVA\ film}$	80 μm
b_{PET}	0.1016 m
b_{sample}	2, 4, 6, 8, 10 cm
R_{roller}	0.0381 m

R2R peeling process. The curvatures K_2 and K_3 were obtained based on the bending radius measurements R_a and R_b from the peeling front images as shown in Fig. 5(a). It was found that all the elastic strains (ε_i, $i = 1, 2, 3$) due to tension were substantially smaller than the rest of the terms in Eq. (6). Therefore, the terms of $\varepsilon_3 - \varepsilon_1$, $\varepsilon_2 - \varepsilon_1$, and $\frac{1}{2}\frac{bh_{f2}\Delta d_1}{(1+\varepsilon_1)}E_2(\varepsilon_1^2 - \varepsilon_2^2) + \frac{1}{2}\frac{bh_{f3}\Delta d_1}{(1+\varepsilon_1)}E_3(\varepsilon_1^2 - \varepsilon_3^2)$ in the equation were ignored. In addition, a baseline constant was subtracted from the strain energy to compensate for the friction effect in the R2R system. This baseline constant was obtained by running the R2R system without peeling graphene samples. Although the adhesion energy is plotted for the entire duration of the experimental run in Fig. 5(c), only region C provides meaningful adhesion energy estimation, because it is the only region with stable peeling. All other regions are affected by disturbances such as sudden release of elastic energy due to the start and end of the peeling process.

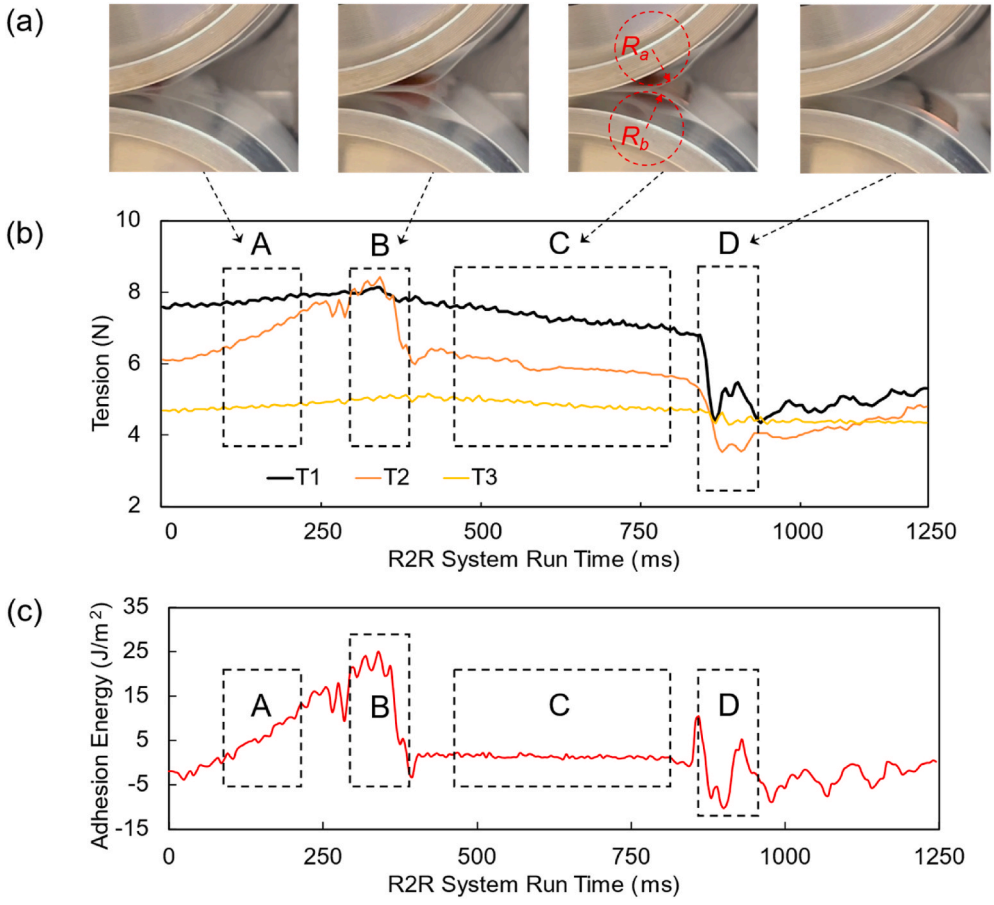

Fig. 5. (a) R2R peeling front progression of a graphene sample of 8 cm wide, (b) real-time tension measurements during peeling, and (c) the adhesion energy estimation. (A colour version of this figure can be viewed online.)

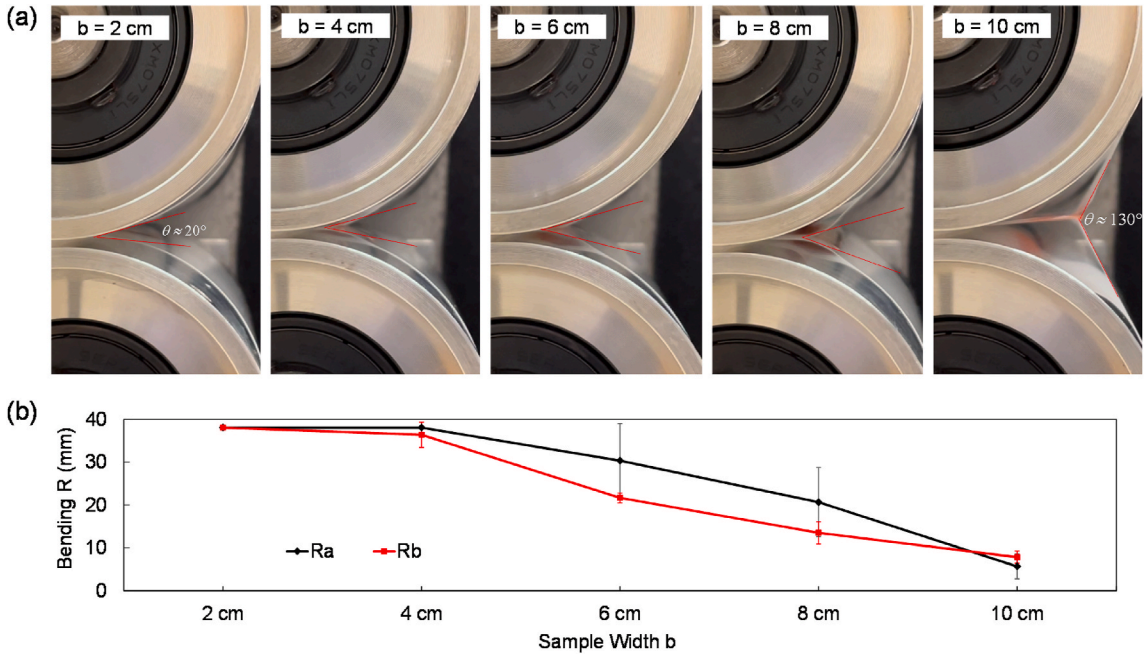

Fig. 6. (a) R2R peeling front geometry at different graphene sample widths, and (b) corresponding bending radius measurements. (A colour version of this figure can be viewed online.)

4.2. Effects of film bending on adhesion energy estimation

The effect of film bending on the adhesion energy estimation was investigated using graphene samples of different widths. Although the same tension force of 5 N was used throughout this study, wider samples generated more bending (Fig. 6(a)) in the two peeled web sections. The digital images were used to measure the bending radius during the peeling process. Fig. 6(b) shows the results of bending radius measurements. When the sample width was small, such as 2 cm and 4 cm, graphene was readily peeled from the copper substrate and almost no additional film bending beyond the curvature of the guiding rollers was observable. When the sample width became larger, in the cases of 6, 8, and 10 cm, the peeling front location shifted away from the nipping point of the two guiding rollers. Larger curvatures resulted in each arm, leading to greater bending effects.

The adhesion energy estimation as a function of sample width is shown in Fig. 7. Fig. 7(a) shows the work done by the external tension forces (U_2). Correspondingly, Fig. 7(b) shows the strain energy due to bending (U_4). As discussed previously, the energy change due to tensile strains (U_3) was negligible. Fig. 7(c) shows the adhesion energy estimation without accounting for the bending effect, whereas Fig. 7(d) shows that with the bending effect accounted. As can be seen from Fig. 7(c), if the bending effect was not accounted, the estimated adhesion energy was as high as 100 J/m^2, almost two orders of magnitude higher than those reported previously [16–21]. Such a high value indicates that the strain energy due to bending (U_4) plays a significant role in measuring the adhesion energy and cannot be ignored. After accounting for the bending effect, the adhesion energy was found to be between 1.22 J/m^2 and 2.58 J/m^2, agreeing well with previous studies. Table 2 summarizes the estimated adhesion energy under different sample width conditions. Three samples were measured under each condition.

As seen in Table 2, the experimental results in this study suggested dependency of the adhesion energy on the graphene sample width. The adhesion energy initially decreased as the sample width increased from

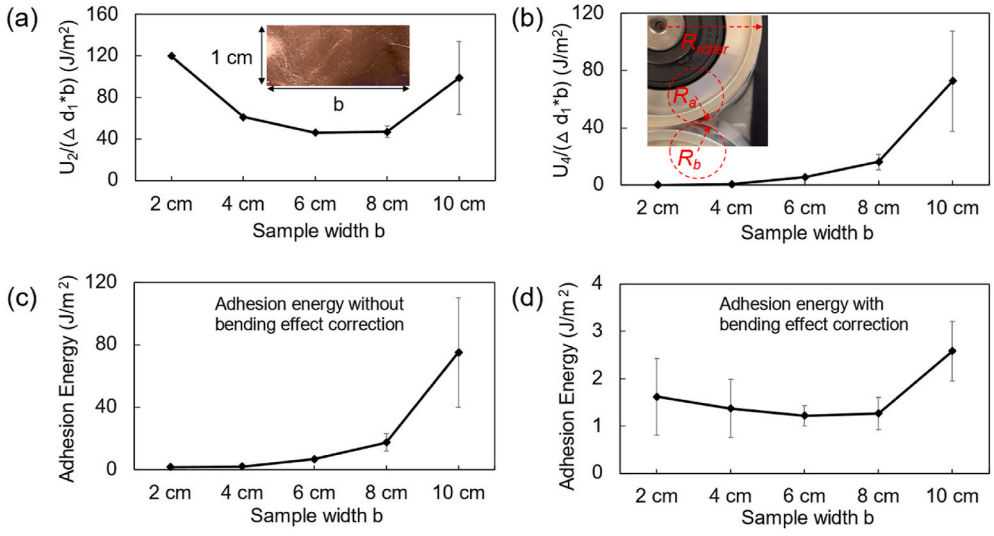

Fig. 7. (a) Plot of $U_2/(\Delta d_1 * b)$, where U_2 is the potential energy changes due to the work done by the external tension forces. The image in the figure shows the dimension of the graphene-on-copper sample. (b) Plot of $U_4/(\Delta d_1 * b)$, where U_4 is the bending energy change during the peeling process. The image shows the measurement of the bending radii. (c) Adhesion energy without the bending effect correction. (d) Adhesion energy with the bending effect correction. (A colour version of this figure can be viewed online.)

Table 2
Adhesion energy estimates.

Sample width (cm)	Average adhesion energy (J/m^2)	±Standard deviation (J/m^2)
2	1.62	±0.81
4	1.37	±0.61
6	1.22	±0.21
8	1.27	±0.34
10	2.58	±0.63

2 cm to 8 cm. It then almost doubled when the sample width increased to 10 cm. This change is caused by the difference in the peeling front geometry. As seen in Fig. 6(a), when the sample width increased from 2 cm to 10 cm, the peeling angle θ increased from approximately 20°–130°. From a fracture mode-mix perspective, interfacial toughness often increases with the shear component of the interfacial traction [24–26]. The shear component decreases as the peeling angle increases when the peeling angle is smaller than 90°. Beyond 90°, the shear component will increase. The adhesion energy trend observed in this study in general is consistent with the fracture mode-mix understanding. However, the relationship between the adhesion energy and peeling angle in the R2R transfer process may be complex and require further investigation in a future study.

5. Conclusion

In summary, a novel method for estimating the adhesion energy of as-grown graphene in a R2R dry transfer process is developed. An energy balance model is established to obtain the adhesion energy based on web tension and bending curvature measurements before and after the peeling point. It is found that the film bending effect is a major factor in the strain energy change during the R2R dry transfer process, and thus needs to be corrected in adhesion energy estimation. After the bending energy correction, the adhesion energy of as-grown graphene on copper foil is estimated to be from 1.22 J/m^2 to 2.58 J/m^2 depending on the peeling angle. The method developed in this study provides a unique approach to estimating the adhesion energy of as-grown graphene with a roller configuration. It enables the monitoring and controlling the quality of transferred graphene using in-process tension measurements in the R2R dry transfer process and paves the way for large-scale graphene applications in multifunctional materials such as those that are both optically transparent and electrically conductive for organic solar cells.

CRediT authorship contribution statement

Nan Hong: Writing - original draft, conceived the idea and designed the experiments, designed and built the R2R testbed and implemented the tension and speed control, performed the experiments, developed the model, wrote the manuscript. Qishen Zhao: conceived the idea and designed the experiments, designed and built the R2R testbed and implemented the tension and speed control, performed the experiments, developed the model, analyzed the data. Dongmei Chen: designed and built the R2R testbed and implemented the tension and speed control. Kenneth M. Liechti: analyzed the data. All authors discussed the results and provided comments on the manuscript. Wei Li: Writing - original draft, conceived the idea and designed the experiments, designed and built the R2R testbed and implemented the tension and speed control, developed the model, analyzed the data, wrote the manuscript.

Declaration of competing interest

The authors declare that they have no known competing financial interests or personal relationships that could have appeared to influence the work reported in this paper.

Acknowledgments

This work is based upon work supported primarily by the National Science Foundation under Cooperative Agreement No. EEC-1160494 and CMMI-2041470. Any opinions, findings and conclusions or recommendations expressed in this material are those of the author(s) and do not necessarily reflect the views of the National Science Foundation.

Appendix A. Supplementary data

Supplementary data to this article can be found online at https://doi.org/10.1016/j.carbon.2022.08.062.

References

[1] L. Banszerus, M. Schmitz, S. Engels, J. Dauber, M. Oellers, F. Haupt, et al., Ultrahigh-mobility graphene devices from chemical vapor deposition on reusable copper, Sci. Adv. 1 (6) (2015) e1500222, https://doi.org/10.1126/sciadv.1500222.
[2] X. Li, W. Cai, L. Colombo, R.S. Ruoff, Evolution of graphene growth on Ni and Cu by Carbon isotope labeling, Nano Lett. 9 (12) (2009) 4268–4272, https://doi.org/10.1021/nl902515k.
[3] B. Lee, W. Chu, W. Li, Effects of process parameters on graphene growth via low-pressure chemical vapor deposition, J. Micro Nano-Manufacturing 8 (3) (2020), https://doi.org/10.1115/1.4048494.
[4] Y. Zhang, L. Gomez, F.N. Ishikawa, A. Madaria, K. Ryu, C. Wang, et al., Comparison of graphene growth on single-Crystalline and polycrystalline Ni by chemical vapor deposition, J. Phys. Chem. Lett. 1 (20) (2010) 3101–3107, https://doi.org/10.1021/jz1011466.
[5] K.S. Kim, Y. Zhao, H. Jang, S.Y. Lee, J.M. Kim, K.S. Kim, et al., Large-scale pattern growth of graphene films for stretchable transparent electrodes, Nature 457 (7230) (2009) 706–710, https://doi.org/10.1038/nature07719.
[6] T. Hesjedal, Continuous roll-to-roll growth of graphene films by chemical vapor deposition, Appl. Phys. Lett. 98 (13) (2011), 133106, https://doi.org/10.1063/1.3573866.
[7] I. Vlassiouk, P. Fulvio, H. Meyer, N. Lavrik, S. Dai, P. Datskos, et al., Large scale atmospheric pressure chemical vapor deposition of graphene, Carbon 54 (2013) 58–67, https://doi.org/10.1016/j.carbon.2012.11.003.
[8] H. Xin, Q. Zhao, D. Chen, W. Li, Roll-to-Roll mechanical peeling for dry transfer of chemical vapor deposition graphene, J. Micro Nano-Manufacturing 6 (3) (2018), https://doi.org/10.1115/1.4040449.
[9] Q. Zhao, N. Hong, D. Chen, W. Li, Controlling peeling front geometry in a roll-to-roll thin film transfer process, in: ASME 2020 15th International Manufacturing Science and Engineering Conference, vol. 2020, 2020, https://doi.org/10.1115/msec2020-8507.
[10] Q. Zhao, N. Hong, D. Chen, W. Li, A dynamic system model for roll-to-roll dry transfer of two-dimensional materials and printed electronics, J. Dyn. Syst. Meas. Control 144 (7) (2022), https://doi.org/10.1115/1.4054187.
[11] N. Hong, D. Kireev, Q. Zhao, D. Chen, D. Akinwande, W. Li, Roll-to-Roll dry transfer of large-scale graphene, Adv. Mater. 34 (3) (2022), 2106615, https://doi.org/10.1002/adma.202106615.
[12] B. Jang, C.-H. Kim, S.T. Choi, K.-S. Kim, K.-S. Kim, H.-J. Lee, et al., Damage mitigation in roll-to-roll transfer of CVD-graphene to flexible substrates, 2D Mater. 4 (2) (2017), 024002, https://doi.org/10.1088/2053-1583/aa57fa.
[13] T. Kobayashi, M. Bando, N. Kimura, K. Shimizu, K. Kadono, N. Umezu, et al., Production of a 100-m-long high-quality graphene transparent conductive film by roll-to-roll chemical vapor deposition and transfer process, Appl. Phys. Lett. 102 (2) (2013), 023112, https://doi.org/10.1063/1.4776707.
[14] S. Bae, H. Kim, Y. Lee, X. Xu, J.-S. Park, Y. Zheng, et al., Roll-to-roll production of 30-inch graphene films for transparent electrodes, Nat. Nanotechnol. 5 (8) (2010) 574–578, https://doi.org/10.1038/nnano.2010.132.
[15] L. Gao, W. Ren, H. Xu, L. Jin, Z. Wang, T. Ma, et al., Repeated growth and bubbling transfer of graphene with millimetre-size single-crystal grains using platinum, Nat. Commun. 3 (1) (2012) 699, https://doi.org/10.1038/ncomms1702.
[16] T. Yoon, W.C. Shin, T.Y. Kim, J.H. Mun, T.-S. Kim, B.J. Cho, Direct measurement of adhesion energy of monolayer graphene as-grown on copper and its application to renewable transfer process, Nano Lett. 12 (3) (2012) 1448–1452, https://doi.org/10.1021/nl204123h.
[17] S.R. Na, J.W. Suk, L. Tao, D. Akinwande, R.S. Ruoff, R. Huang, et al., Selective mechanical transfer of graphene from seed copper foil using rate effects, ACS Nano 9 (2) (2015) 1325–1335, https://doi.org/10.1021/nn505178g.
[18] S.R. Na, S. Rahimi, L. Tao, H. Chou, S.K. Ameri, D. Akinwande, et al., Clean graphene interfaces by selective dry transfer for large area silicon integration, Nanoscale 8 (14) (2016) 7523–7533, https://doi.org/10.1039/C5NR06637A.
[19] S. Das, D. Lahiri, D.-Y. Lee, A. Agarwal, W. Choi, Measurements of the adhesion energy of graphene to metallic substrates, Carbon 59 (2013) 121–129, https://doi.org/10.1016/j.carbon.2013.02.063.
[20] Z. Cao, P. Wang, W. Gao, L. Tao, J.W. Suk, R.S. Ruoff, et al., A blister test for interfacial adhesion of large-scale transferred graphene, Carbon 69 (2014) 390–400, https://doi.org/10.1016/j.carbon.2013.12.041.

[21] H. Xin, R. Borduin, W. Jiang, K.M. Liechti, W. Li, Adhesion energy of as-grown graphene on copper foil with a blister test, Carbon 123 (2017) 243–249, https://doi.org/10.1016/j.carbon.2017.07.053.
[22] L. He, J. Lou, S. Kitipornchai, J. Yang, J. Du, Peeling mechanics of hyperelastic beams: bending effect, Int. J. Solid Struct. 167 (2019) 184–191, https://doi.org/10.1016/j.ijsolstr.2019.03.011.
[23] A. Ugural, S. Fenseter, Advanced Mechanics of Materials and Applied Elasticity, sixth ed., Pearson, 2019.
[24] K.M. Liechti, Y.S. Chai, Asymmetric shielding in interfacial fracture under in-plane shear, J. Appl. Mech. 59 (2) (1992) 295–304, https://doi.org/10.1115/1.2899520.
[25] A.G. Evans, M. Rühle, B.J. Dalgleish, P.G. Charalambides, The fracture energy of bimaterial interfaces, Metall. Trans. A 21 (9) (1990) 2419–2429, https://doi.org/10.1007/BF02646986.
[26] J.S. Wang, Z. Suo, Experimental determination of interfacial toughness curves using Brazil-nut-sandwiches, Acta Metall. Mater. 38 (7) (1990) 1279–1290, https://doi.org/10.1016/0956-7151(90)90200-Z.